Water thin film-silica interaction on α-quartz (0001) surfaces

Yun-Wen Chen, Iek-Heng Chu, Yan Wang, and Hai-Ping Cheng

Phys. Rev. B **84**, 155444 — Published 28 October 2011

DOI: 10.1103/PhysRevB.84.155444

Water thin film-silica interaction on α-quartz (0001) surfaces

Yun-Wen Chen, Iek-Heng Chu, Yan Wang, and Hai-Ping Cheng

Department of Physics and the Quantum Theory Project

University of Florida, Gainesville, FL 32611

Abstract

Interactions between thin water films and α-quartz (0001) surfaces are studied using first-principles density functional theory calculations. Layer-by-layer water deposition with up to five layers of water film on both bare and fully hydroxylated α-quartz (0001) surfaces is examined. Except for water monolayer adsorption, the interactions between water and bare quartz surfaces with Si-O-Si terminations are found to be relatively weak, with adsorption energies similar to the hydrogen bonding strength. However, the interactions between water and surfaces with hydroxyl terminations are much stronger, with a film-surface bonding energy an order of magnitude larger than on bare surfaces. A stable bilayer configuration is identified on all surfaces. In particular it shields the water-silica interaction effectively and makes a surface inert to water molecules. Examination of lateral translation of water thin films on bare surfaces supports the results of friction experiments.

I. INTRODUCTION

The water-silica interface interaction continues to attract considerable attention in a wide range of scientific communities because of its ubiquity in biological and environmental sciences, technology, and daily life [1, 2]. For example, silica is the major constituent of diatom cell walls which are constructed by complex chemical processes involving silica, water, and other reactants. The amazing structure of such cell walls not only draws the attention of biologists but also stimulates studies of its application in nanotechnology [3]. Another remarkable example is silica-based DNA/RNA sequencing technology. The capillary electrophoresis is done by solution confinement within silica channels [4-6].

There have been numerous experimental studies on the mechanism of hydroxylation of silica surfaces, water adsorption on silica surfaces, and water confinement in silica nanopores. Asay and Kim studied water layers adsorbed on a hydroxylated silica surface with attenuated total reflection-infrared spectroscopy at different degrees of humidity [7]. They suggested that the adsorbed water forms an ice-like network on the surface that propagates up to ~3 layers at room temperature. Optiz et al. measured the friction force of a water thin film on silica surfaces with scanning force microscopy (SFM) technique [8]. Those measurements showed dramatically different tendencies between hydroxylated and bare surfaces, with high and low friction forces respectively. Ostroverkhov and Shen et al. studied a series of phase-sensitive sum-frequency spectroscopies of the water-quartz interface and analyzed the icelike and

liquidlike peaks in the spectrum and the net polar orientation of water at the interface under different pH environments [9, 10]. They then suggested that the liquidlike peaks are from water molecules being adsorbed at more easily deprotonated sites. However, the explanation is still speculative since the measurement represents only the effect of net polar-oriented molecules, not the total number of contributing molecules. The molecular picture needs to be confirmed by molecular dynamics simulations as pointed out in a review article by Shen and Ostroverkhov[10]. The system of water confined in silica nanopores was studied by many groups [11, 12]. The melting and freezing temperatures of confined water were measured with respect to different pore size and filling fraction. In the theoretical model [13], the size of the nanopores and the thickness of the non-freezing bound water layer next to the silica wall will affect the melting and freezing temperatures of core water. Liu et al., suggested that a bilayer water film will be formed once the pore wall is completely covered with adsorbed water [12].

The experimental observations provide rich information that could reveal the properties like hydrophile, dielectric constant, and friction at the water-silica interface. However, a clear molecular picture of the interface needs the cooperation of experiments and molecular simulations as recommended, for example, by Feibelman in a review paper of water on a solid [14]. Very recently, Feibelman et al. have investigated the water thin-film adsorption on Pt (111) surfaces via molecular simulations, and got good agreement with experiments [15-17].

Multiple theoretical investigations have been done via density functional theory (DFT) or classical molecular dynamics (MD) methods. Du et al. studied the hydroxylation of two-membered ring sites on the amorphous silica surface with a combination of classical MD and DFT calculations[18]. They observed a barrier-free double hydrogen atom transfer process when there were two water molecules interacting with a two-membered ring site. Du et al. [19] and Adeagbo et al. [20] simulated water molecules interacting with fully hydroxylated α-quartz (0001) surfaces. The dissolution of a $Si(OH)_4$ unit on the surface was studied as well and it was concluded that the dissolution of a $Si(OH)_4$ unit may not occur spontaneously. Du et al. [21] and Rignanese et al. [22] showed that the perfectly reconstructed α-quartz (0001) surface is fairly resistant to attack by water. Further, Rignanese et al. showed this surface is also very hard to be hydroxylated [22].

Confined water in a silica pore was simulated using classical MD [23-25]. Rovere et al. [23]and Gallo et al. [24] analyzed the layer structure of water. They both found that water layers formed near the silica wall and the structure converged to bulk water near the center of silica pore. In their simulation, Moore et al. reported [25] that the freezing and melting temperatures match well with experimental observation, and a 2 : 1 ratio of cubic to hexagonal layers in the confined ice was observed.

The adsorption of water layers on a silica surface was studied by DFT and classical MD calculations as well. Yang et al. found water could form an icelike layer on fully hydroxylated β-cristobalite (100) and α-quartz (0001) surfaces in

their DFT calculations [26, 27]. The icelike water layer formed hydrogen bonds with the hydroxyl group on the surfaces, with all hydrogen bonds saturated. The average adsorption energies are comparable with the hydrogen bonds within Ice XI bulk. Several groups studied the density distribution, dipole orientation, and drift velocity of water molecules in bulk water adsorbed on silica surfaces using classical MD [28-30]. Argris et al. showed that hydroxylation conditions can greatly alter the behavior of water molecules in those distributions [29].

In a previous study, we reported first-principles calculations on thin water films up to four monolayers on quartz (0001) surfaces [31]. We found that in going from a water monolayer to multilayer, the low energy state configurations and adsorption sites showed a transition due to formation of a highly stable bilayer membrane-like structure. Here, we report a systematic computational investigation of the adsorption of water thin films on the α-quartz (0001) surfaces. Water was added layer by layer. Water layers with two different orientations adsorbed on bare surfaces are discussed. Conversely, only one kind of water layer orientation adsorption was studied on hydroxyl terminated surfaces for the strong interaction between hydroxyl groups and water molecules. Furthermore, we find that the friction of a water thin film is small on bare surfaces, consistent with the experimental observations by Opitz et al.[8].

The rest of the paper is organized as follows. In Section II, we discuss the model and parameters used in our calculations. Then we present our calculated results for water mono-, bi-, tri-, and quad-layer adsorption on surfaces in Section III where we discuss the adsorption geometries, the bonding and adsorption

energies, as well as the charge transfer of different adsorption states on surfaces. In Section IV, we show variations of the total energy with respect to the lateral displacements of water thin films on bare surfaces. In Section V, we discuss the effect of van der Waals force applying on our simulation systems. Finally we summarize our results and draw conclusions in Section VI.

II. METHOD AND CALCULATION DETAILS

The electronic structure calculations were performed using density functional theory as implemented in the Vienna ab initio simulation package (VASP) [32] . The projector augmented wave (PAW) [33] technique in conjunction with the plane wave basis set and the Perdew-Wang generalized gradient approximation (PW91) [34] of the exchange and correlation functional were employed in all simulations. A 2×2×1 Γ centered Monkhorst-Pack k-point mesh [35] in Brillouin zone and 400 eV kinetic energy cutoff for plane-wave basis-set were used to ensure energy convergence. The structures were optimized with a global break condition that the force on each atom is less than 0.01 eV/Å.

The simulated systems consist of silica α-quartz (0001) surface slabs and water thin films. Three kinds of surfaces were included in this study, bare (perfect reconstructed) surfaces with (1×1) and (2×1) symmetry [36-38] (Fig 1(a) and (b)), and a fully hydroxylated surface [27, 39] (Fig 1(c)). The bare surfaces have Si-O-Si terminations, the same termination as the bare amorphous surface in the study by Opitz et al. [8] For convenience, they are denoted as surface I, II, and III

respectively in the following text. Each surface is modeled by a slab containing 2 × 2 × 5 α-quartz unit cells in a periodic hexagonal supercell (9.9 Å × 9.9 Å × 77.2 Å) with one central unit cell fixed at the optimized bulk structure. To eliminate surface dipoles, the water films are adsorbed symmetrically on the top and bottom surfaces. The separation between two adjacent slab images is set to be 50 Å to make the interaction between the water layers on the two surfaces of a silica slab negligible under periodic boundary condition.

In our previous study, we found that there are two kinds of water molecule adsorption sites on both (1x1) and (2x1) bare surfaces (surface I and II) [40]. One is a silicon atom (atop) site, while the other is hollow site which is the center of a six-membered ring on the surfaces. On surface I, all of the atop sites form a hexagonal 2D array which matches the hexagonal geometry of Ice XI (0001) surface (basal plane). On the other hand, all of the hollow sites in combination with half of the atop sites also form the same array (Fig .1). Surface II is another perfectly reconstructed surface that has lower surface energy than surface I. The two surfaces can transform from one to another via rotations of surface SiO_4 terahedral units and thus have the same topological structure[38]. All atop sites on surface II form a twisted 2D hexagonal array.

On two bare surfaces, the water monolayer with the structure of one Ice XI basal plane sublayer is added one by one on top of the surfaces. Two kinds of water monolayer orientations were considered. One has the out-of-plane protons pointing up and the other pointing down. We call the adsorption type of water monolayer with protons pointing up a H-up state. Similarly, the water monolayer

adsorption with protons pointing down is defined as a H-down state. On the fully hydroxylated surface, only the H-down state adsorption is present for the strong hydrogen bonds forming between water layer and the hydroxyl groups on the surface.

In each system, we calculate the adsorption energy as well as the bonding energy in order to clearly describe the features of water film adsorption on silica surfaces. The adsorption energy of *n*th water layer is defined as

$$E_n^a = -(E_{total}(n) - E_{total}(n-1) - mE_{H_2O})/area, \quad (1)$$

where $E_{total}(n)$ is the total energy of the system with n water layers adsorbed on the surface, E_{H_2O} is the energy of one freestanding water molecule, *m* is the number of water molecules in one water layer (8 in our simulation systems). Surface area is equal to 84.9 $Å^2$ for one side of a surface slab. The corresponding total adsorption energy per water molecule for *n* water layers is defined as

$$E_n^{a\prime} = -(E_{total}(n) - E_{surface} - n * mE_{H_2O})/(nm), \quad (2)$$

The bonding energy of *n* water layers to surface is defined as

$$E_n^b = -(E_{total}(n) - E_{surface} - E_{n-H_2O-layer})/area, \quad (3)$$

where $E_{subsystem}$ is the energy of the individual surface or water layer(s) subsystem having the same configuration of relaxed total system. Thus by definition, the adsorption energy includes the water-silica interaction and the

hydrogen bond interaction within water layers. The bonding energy only includes the interaction between the water entity and the silica surface. However, the deformation energy (from the optimized configuration) of each subsystem is not counted in the bonding energy.

The charge density difference is defined as

$$\Delta\rho(\boldsymbol{r}) = \rho(\boldsymbol{r}) - \rho_{surface}(\boldsymbol{r}) - \rho_{n-H_2O-layer}(\boldsymbol{r}), \quad (4)$$

where $\rho(\boldsymbol{r})$, $\rho_{surface}(\boldsymbol{r})$, and $\rho_{n-H_2O-layer}(\boldsymbol{r})$ are the total charge density of the optimized system, the charge density of the pure surface, and the charge density of the free-standing water thin film, respectively. We also calculate the charge redistribution in the system, defined as

$$\int |\Delta\rho(\boldsymbol{r})|\, d^3r = \frac{\sum_{i,j,k}|\Delta\rho_{i,j,k}|}{total\ grids}, \quad (5)$$

where the indices i, j and k are indices of real space grids of three supercell vectors in DFT calculations, respectively. Charge transfer from surface to water is calculated by using a real-space Bader charge analysis [41, 42].

III. WATER ADSORPTION ON SURFACES

A. Water monolayer adsorption

In Fig. 2, we show the optimized structures of a water monolayer adsorbed on surface I in two distinct adsorption states. One has its out-of-plane hydrogen pointing up (H-up state, Fig. 2 (a) – (d)) and the other pointing down (H-down

state, Fig. 2 (e) – (h)). Each of the two relaxed water monolayers adsorbed on this surface has a flat-ice structure with two groups of hydrogen bond lengths (~1.75 Å and ~1.96 Å). Because of lattice mismatch, the ice layer is stretched laterally and therefore is flat compared to that in the bulk ice. For the H-up state on surface I, the water molecules prefer to be adsorbed on all atop sites of the surface. For the H-down state, half of the water molecules with a proton pointing down will be adsorbed on the hollow sites of the surface, while the other half are adsorbed on the atop sites. The ground state is the H-down state, which has a total surface energy lower than the H-up state by 1.79 meV/Å^2.

On surface II, the ground state is still the H-down state, which is more stable than H-up state by an energy difference of 1.71 meV/Å^2. As compared to the counterparts on surface I, each water monolayer is slightly deformed, with a larger variation on the longer hydrogen bond group (1.93 ~ 2.01 Å for H-up state, 1.95~1.98 Å for H-down state) on surface II. The distance between the water layer and silica surface is 3.61 Å for the H-up state and 3.17 Å for the H-down state. Both are larger than the corresponding cases on surface I. The oxygen atoms of water molecules atop the silicon atoms are slightly away from the true atop sites in order to retain the hexagonal icelike structure. In our calculations, the distance of the water thin-film to surface for H-down states is smaller (3.0 to 3.2 Å) than for H-up states (3.3 to 3.6 Å) on surface I and II in monolayer and multilayer cases.

Surface III is a fully hydroxylated α-quartz (0001) surface with (1x1) symmetry, which has been also studied by Murashov [39] and Yang et al. [27] by using

DFT calculations. The hydroxyl groups form hydrogen bond chains within the surface, with alternative strong and weak bond strength [27]. When water molecules are adsorbed on surface III, the interaction of the hydroxyl groups with water molecules is very strong ($E_1^{a\prime}$ =659.8 meV/molecule) and comparable with hydrogen bonds between water molecules in Ice XI bulk (~710 meV/molecule in DFT [43], ~610meV/ molecule in experiment [44]). The one-water molecule adsorption on the surface has an adsorption energy of 618.9 meV (543 meV in Ref. 27). Because of the strong hydrogen bond between water thin-film and surface, the water monolayer will be adsorbed in H-down state as reported by Yang et al. [27] Each water molecule will form one hydrogen bond with the hydroxyl group on silica surface, as shown in Fig. 3. This type of water monolayer adsorption will fully saturate the hydrogen bonds of water molecules and hydroxyl groups on the surface (Fig. 3). In our calculation, we also find that there are another two H-down states with similar total energy as the one shown in Fig. 3 (difference within 1 meV/ Å^2) but with 120º rotation difference in the X-Y plane.

B. Water bilayer adsorption

When a second layer of water is added onto surface I, the low energy state becomes to the H-up state instead of the H-down state. We find that, in both cases, the second Ice XI sublayer deposited on top of the first water layer prefers an optimized structure with the out-of-plane protons pointing downward, as shown in Fig. 4 (a) and (b). The out-of-plane protons in the second monolayer of the H-up state reverse the orientations (from pointing upward to downward), but a similar phenomenon does not happen in the H-down state. As a result, the two

water layers form a membrane-like bilayer film in the H-up state, and all hydrogen bonds of the water are saturated within the water entity. The total surface energy difference between the H-up and H-down states is 18.9 meV/Å^2, which is much larger than the case with water monolayer adsorption, as shown in Fig. 5. The total adsorption energies, $E_1^a{}'$, are 599.5 and 499.0 meV/ molecule for H-up and H-down states, respectively. For the H-up state this adsorption energy is only about 15% (or ~100 meV/molecule) smaller than the calculated cohesive energy of a water molecule in bulk ice-XI, which is 702.2 meV/molecule. The formation of hydrogen bonds in the membrane-like water bilayer film in the H-up state contributes a large amount to the total surface energy and the adsorption energy, thus the H-up state becomes more stable than the H-down state. This point will be discussed in the Section III-D, where we analyze the adsorption and bonding energies tendency as the number of water layers is growing.

Similar to the case of surface I, the ground state of water bilayer adsorption on surface II is the H-up state. The water bilayer forms a membrane-like structure as well. This water bilayer on surface II is very similar to its counterparts on surface I with much smaller deviations between them than that between water monolayer adsorption cases on surface I and II.

When the second water layer is deposited on surface III, the structure of the first water is almost stationary and the hydrogen bonds between the first and second water layer are relatively long (about 2 Å) (Fig. 4 (c)). The bonding energy between two water layers is only 5.8 meV/ Å^2, indicating that the

interaction between the two water layers is relatively weak and that the first water layer effectively shields the long-range surface water interaction.

We note that complicated water structures may form on surfaces [15, 16] and artificial results may be obtained when the size of supercell in simulations is too small. Therefore, we examine the size issue using classical molecular dynamics (MD) simulations as implemented in DL_POLY package [45] with CLAYFF force field [46]. The CLAFF force field for water is modified from the SPC water model, and we have tested the cohesive energy of Ice XI to be 615.8 meV/molecule in this model. We test the system stability of water monolayer, bilayer in H-up, and H-down states on surface I and water monolayer on surface III with a MD cell that consists of 10x10 unit cells in X-Y plane. During the simulations, the temperature of the system is increasing from 10K to 300K with a rate of 10K/4ps. The overall simulation time is 120 ps, with a time step equal to 0.2 fs. The results confirm that these structures are stable in the extended supercell. It is also observed that the membrane-like water bilayer (H-up state) on surface I and the monolayer on surface III are very stable up to 120K. Systems with various disordered water films (obtained at simulated temperatures higher than 120 K) do not recover the hexagonal bilayer structure when they are annealed down to 0 K (due to limited annealing time), and their total energies are always higher than that of the hexagonal bilayer structure. Even though there are many possibilities that water molecules could form more stable large-scale structure other than our proposed models, our DFT calculations based on a few selected stable isomer structures catch the general features of water-silica interaction.

C. Water multilayer adsorption

Continue to add water layers on bare quartz surfaces, we find that the H-up states is always more stable than H-down states up to four water layers. In Fig. 5, we show the total energy difference between H-up and H-down states on surface I and II up to water quadlayer adsorption. Generally the total energy difference increases as the number of water layers increases, except for the case of water trilayer adsorption. We confirm this trend by calculating the case with pentalayer adsorption on surface I, which shows a further increased energy difference of 29 meV/ $Å^2$. In Fig. 6, we show the structures of water trilayer and quadlayer adsorption on surface I. When the third water layer is added on top of the H-up bilayer structure, some hydrogen bonds break in the second water layer and some hydrogen bonds form between the second and third water layers, as shown in Fig. 6 (a). As a result, the water layers pucker in the vertical direction. When the fourth water layer is added with the H-up state, the third and fourth water will form hydrogen bonds between each other and they pucker in a larger range than the first water layer. As compared with the case of water trilayer adsorption, the first and second water layers are almost stationary after the fourth water layer is adsorbed. For the H-down state, the first two water layers are almost stationary and the third and fourth water layer forms hydrogen bonds with the previous water layer. The result is like a piece of Ice XI placed on a silica surface, as shown in Fig. 6 (b) and (d).

On surface II, the water multilayer adsorptions show similar results as on surface I. The structures of the water trilayers and quadlayer in H-up and H-down states deviate slightly from the counterparts on surface I.

When the third water layer is deposited onto the water bilayer on surface III, the out of plane protons in the second water layer reverse their orientations from pointing down to up. As a result, the optimized structure consists of two membrane-like bilayers: surface-the first layer structure and water bilayer structure (Fig. 7 (a)). When the fourth water layer is deposited onto the two membrane-like bilayer structures, a trilayer structure similar to the one on surface I and II is obtained (Fig. 7 (b)). Results of trilayer and quadlayer adsorptions on surface III confirm that the bilayer-like structure at the silica-water interface effectively shields the interaction between the hydroxyl groups on the silica surface and water layers beyond the first layer.

D. Bonding and Adsorption energies

In Table 1A and 1B we show the adsorption and bonding energies of water layers adsorption on surfaces in H-up and H-down states, respectively. On surface I and II, the bonding energies of H-up states are around 1.4 to 1.6 meV/Å^2, which are much smaller than that of the H-down states adsorption energies (2.7 to 6.3 meV/ Å^2). The bonding energies on surface III are typically about 35 meV/ Å^2, which is much stronger than all cases on bare surfaces. Except for the quadlayer, pentalayer in H-down states on surface I and II, the bonding energies are very stationary with respect to the increasing of water

layers. This indicates that the water-silica interaction is mainly from the water-silica interface; the surfaces are effectively shielded by the first two water layers.

In the H-down states, we did not observe the flipping of out-of-plane hydrogen atoms as what happened in the H-up states when there are more than two water layers adsorbed. As comparing to the H-up state, the stronger bonding energy in H-down states could be the reason for preventing the flipping of out-of-plane hydrogen atoms. In H-down states, the bonding energies are always smaller on surface II than surface I. The reason could be because surface II is more stable than surface I [38]. However, the same phenomena are observed in H-up states only for monolayer and bilayer adsorptions, but not for trilayer and quadlayer. The reason may be that the energy difference is close to the error bar in calculations. One interesting phenomena is the bonding energies of H-down state on surface I and II are steeply rising at quadlayer adsorption. There is a corresponding large charge transfer at quadlayer adsorption as well, and we will discuss it in the next section.

On surfaces I and II, the adsorption energies of water layers are on the order of 43 to 69 meV/ Å^2 for E_n^a, or 456-732 meV/molecule for $E_n^a{}'$. These numbers are comparable to the hydrogen bonds in the Ice-XI bulk (~710 meV/ molecule in DFT calculations [43]) and much larger than the bonding energies calculated via Eq. (3). So the major contributions to the adsorption energies are from hydrogen bonds of the water films; the water-silica interaction is much smaller than the strength of hydrogen bonds in water. In H-up states, E_2^a is the largest for all hydrogen bonds being saturated in water bilayer adsorption; E_3^a and

E_4^a are relatively small because there are unsaturated hydrogen bonds in monolayer, trilayer, and quadlayer adsorptions. In H-down states on surfaces I and II, the adsorption energies are slightly rising in quadlayer adsorption case (and pentalayer adsorption case on surface I) and it has the same tendency for the bonding energies, E_4^b and E_5^b. E_1^a is smaller than E_2^a and E_3^a because of the energy cost for slight deformation of surfaces when adsorbing the first water layer.

The adsorption energies E_1^a and E_3^a on surface III are especially large because the membrane-like bilayer structures are formed in the water films. In these two cases, all hydrogen bonds have been saturated thus the structures are relatively stable in the energetic point of view.

E. Charge transfer

In Table 2 and Table 3 we show the amount of charge transfer and charge redistribution for H-down states. For H-up states on surface I and II, the numbers are all smaller than 0.01 e^- and 0.1 e^- for charge transfer and charge redistribution, respectively; both are negligible and not listed in the tables. In our calculations, the H-down states have much larger charge transfer and charge redistribution than H-up states. The charge density difference of each H-down state, which is the spatial arrangement of charge redistribution, spreads into larger range than H-up states.

The stronger water-silica interaction does not guarantee a larger charge transfer. On surface III, the charge transfer (Table 2) is not always larger than

that on surface I and II; it is even obviously smaller in the case of water quadlayer adsorption. However, the stronger interaction usually companies with a larger range of charge density difference, and therefore larger charge redistribution. This point is confirmed when comparing Table 1 and Table 3. In Fig. 1, 2 and 3, we show the charge density difference of H-up and H-down water monolayer adsorption on surface I and water monolayer adsorption on surface III. One special feature is that the charge density differences of H-down states always form hexagonal quadrupole array on the surfaces.

In the Section III-D, we show that the bonding energy of H-down state has a steep increase from the trilayer to the quadlayer adsorption. The charge transfer and charge redistribution also show a significant increment from the trilayer to the quadlayer adsorption. The charge density difference is concentrated at the silica-water interface and the top layer of water thin-film, which is shown in Fig. 8 (a). However, this phenomenon does not occur in H-up states as shown in Fig. 8 (b). The charge transfer analysis of H-down states on surface I is summarized in Fig. 9. It requires further investigations to understand the reason for the increment in the bonding energy, the amount of charge transfer, and charge redistribution in the H-down states adsorption on bare surfaces.

IV. SMOOTHNESS OF THE BARE SURFACE

Opitz et al. reported a series of friction measurements of water thin film adsorbed on silica surfaces. They observed that the bare surface with Si-O-Si

appearance had much lower friction force than the hydroxylated surface with hydroxyl appearance. For the bare surfaces, the observed friction force curves are almost the same for various humidity conditions [8]. In contrast, the fully hydroxylated surface had much higher frictional force and its strength fluctuated with increasing humidity [8]. There is little doubt that the water thin film on hydroxylated surface will exhibit high friction resulting from the hydrogen bonds formed between the first water layer and the surface. However, the friction of the water film on the bare surface could be small due to the relatively weak water-silica interaction.

To estimate the smoothness of the bare α-quartz (0001) surface, we calculate the total energy $E_{total}(n)$ of the water thin film as a function of lateral translation on surface I. Because surface I has hexagonal symmetry, we simplify the possible lateral translation into three paths as indicated in Fig. 10 (a). In Fig. 10 (b), (c), and (d), we show the total energy variation curves of three types of water adsorption: monolayer adsorption with H-down and H-up state, and water bilayer with H-up state, respectively. According to the definition of equation (1) and (3), the total energy variation will equal the adsorption and bonding energy variation along the lateral translation as well.

Neglecting the profile detail of the curves, the amplitude of total energy variation in the first case is about ten times larger than in the other two cases. This difference indicates that the friction is strongest in the H-down state of monolayer adsorption. However, in all cases, the maximum total energy variation is small compared to the strength of hydrogen bonds formed between water layer

and hydroxyl groups on surface III (bonding energy is ~ 36 meV/ $Å^2$). It should be noted that use of the simple lateral translation paths without considering geometry optimization is the upper bound (10 meV/ $Å^2$, for H-down state, 1meV/ $Å^2$, for H-up state) of the true total energy variation. In preceding sections we demonstrated that the interaction between the bare silica surface and the water layers above the first water layer is negligible. Thus the adsorption of more water layers will contribute little to the bonding energy. Comparing with the large bonding energy of water thin film adsorbed on surface III (~36 meV/ $Å^2$), our calculations confirmed the observations by Opitz et al. that the friction force of water thin film on bare silica surface is much weaker than on hydroxylated surface [8].

V. Van der Waals force correction

In section III we show that the distance between the water film and the silica surface in the H-up state is larger than 3 Å. The GGA exchange correlation energy functional does not properly describe the long-range dispersion interactions in such loosely bonded systems; therefore the van der Waals (vdW) force correction might be important for studies of water-solid interfaces[47]. In this section, we examine our calculations with the inclusion of vdW corrections and discuss if and how our results are affected.

To evaluate the dispersion effects, we followed the approach proposed by S. Grimme to include the semi-empirical dispersion corrections, which we have

implemented in the Quantum Espresso package [48-50]. We applied these corrections to water monolayer as well as bilayer adsorption on surface I, and water monolayer on surface III (hydroxylated surface). In general, vdW corrections lead to an increase in the interactions between water thin-films and silica surfaces and a decrease in the distances between water thin-films and surfaces by an amount ranging from 0.3 Å to 0.7 Å. However, the structures of water thin-films and the surfaces only change slightly upon structural optimizations. The bonding energies increase by 6 meV/ $Å^2$ and 8 meV/ $Å^2$ for the H-up state and H-down state on surface I, respectively, and by 14 meV/$Å^2$ for the water monolayer on surface III. We also found that the charge transfer between water thin-films increases by a negligible amount, (0.01 |e|) for both H-up and H-down states. On surface I, the ground state is still the H-down state for water monolayer adsorption, and still the H-up state for bilayer adsorption, with a slight change in the total energy difference between H-up and H-down states. We also examined the total energy variation along lateral translations on surface I with the dispersion forces included. The maximum total energy variations become 5 meV/ $Å^2$ and 20 meV/ $Å^2$ for the H-up and H-down states, respectively. However, these values are still much smaller than the bonding energy of water thin-film on fully hydroxylated surface (47 meV/ $Å^2$). According to these results, the presence of the vdW corrections does not change our previous conclusions.

It should also be pointed out that the strength of hydrogen bonds in bulk ice is overestimated by 16% when using GGA functionals (experiment: 610 meV/molecule; DFT-GGA: 710 meV/molecule), and it will be overestimated by a

further 19% when vdW corrections are applied (DFT-GGA-vdW: 825 meV/molecule). In this light, vdW corrections are somewhat controversial here, and it is possible that accurate values of film-surface distance and bonding energy lie somewhere between GGA and GGA+vdW. The important point is that our major conclusions remain unchanged. Further theoretical constructions of GGA potentials might be necessary, but this is not the focus of this work.

VI. CONCLUSION

In summary, the adsorption of water thin film on bare perfectly reconstructed and fully hydroxylated α-quartz (0001) surfaces were studied by using first-principles calculations. Bare surfaces show a contact transition with water thin-film from H-down state in monolayer to H-up state in water multilayers due to the formation of a highly stable water bilayer membrane-like structure. The interaction between the water thin film and a fully hydroxylated surface is much stronger, with 10 times (4 times when the vdW correction is applied) larger water-silica bonding energy than that of the bare surface. The first water layer and the hydroxyl groups of the fully hydroxylated surface also form a membrane-like bilayer structure. For each surface the water-silica interactions are highly localized between the first water layer and the surface due to shielding of the membrane-like bilayer.

Interestingly on bare surfaces, the H-down adsorption configuration is an isomer state when there is more than one adsorbed water layer. A surprising

jump in water-silica interaction strength, that is, the bonding energy, is observed when the thickness of the water film increasing from trilayer to quadlayer with the corresponding increase in charge transfer. The trend continues in water pentalayer adsorption, suggesting a thickness-induced surface process. Whether this transition is caused by the subtleness of long-range interaction or by emerging collective behavior is beyond the scope of this work. Future studies are necessary to investigate the mechanisms for the unexpected sudden jump in water-silica interaction. We also suggest that carefully designed experiments should also be conducted to verify the phenomenon.

The stability of the water adsorption on bare surface also was examined by calculating the total energy variation. For water thin film with H-up state the maximum energy variation along the lateral translation on surface is smaller than 1 meV/ $Å^2$ (5 meV/ $Å^2$ when vdW correction is applied). Our calculations confirm the experimental observations that the friction force of water thin film on bare silica surface is much weaker than on hydroxylated surface [8].

Acknowledgement

The authors would like to express deep appreciation to Professor Samuel B. Trickey for constructive discussion and suggestions. This work was supported by the NSF under Grant No. DMR-0804407. The computing resources were from NERSC and University of Florida/HPC centers.

[1] R. K. Iler, *The Chemistry of Silica Solubility, Polymerization, Colloid and Surface Properties, and Biochemistry* (Wiley, New York, 1979).

[2] A. P. Legrand, *The Surface Properties of Silicas* (John Wiley, Chichester ; New York, 1998).

[3] J. Bradbury, Plos Biology **2**, 1512 (2004).

[4] E. N. Fung and E. S. Yeung, Analytical Chemistry **67**, 1913 (1995).

[5] A. T. Woolley and R. A. Mathies, Analytical Chemistry **67**, 3676 (1995).

[6] D. Schmalzing, A. Adourian, L. Koutny, L. Ziaugra, P. Matsudaira, and D. Ehrlich, Analytical Chemistry **70**, 2303 (1998).

[7] D. B. Asay and S. H. Kim, Journal of Physical Chemistry B **109**, 16760 (2005).

[8] A. Opitz, S. I.-U. Ahmed, J. A. Schaefer, and M. Scherge, Wear **254**, 924 (2003).

[9] V. Ostroverkhov, G. A. Waychunas, and Y. R. Shen, Physical Review Letters **94**, 046102 (2005).

[10] Y. R. Shen and V. Ostroverkhov, Chemical Reviews **106**, 1140 (2006).

[11] G. H. Findenegg, S. Jähnert, D. Akcakayiran, and A. Schreiber, ChemPhysChem **9**, 2651 (2008).

[12] X. X. Liu, Q. Wang, X. F. Huang, S. H. Yang, C. X. Li, X. J. Niu, Q. F. Shi, G. Sun, and K. Q. Lu, Journal of Physical Chemistry B **114**, 4145 (2010).

[13] R. Evans, Journal of Physics-Condensed Matter **2**, 8989 (1990).

[14] P. J. Feibelman, Phys Today **63**, 34 (2010).

[15] P. J. Feibelman, N. C. Bartelt, S. Nie, and K. Thürmer, Journal of Chemical Physics **133**, 154703 (2010).

[16] S. Nie, P. J. Feibelman, N. C. Bartelt, and K. Thürmer, Physical Review Letters **105**, 026102 (2010).

[17] A. Hodgson and S. Haq, Surface Science Reports **64**, 381 (2009).

[18] M. H. Du, A. Kolchin, and H. P. Cheng, Journal of Chemical Physics **119**, 6418 (2003).

[19] Z. M. Du and N. H. de Leeuw, Dalton Transactions, Iss. <22>, 2623 (2006).

[20] W. A. Adeagbo, N. L. Doltsinis, K. Klevakina, and J. Renner, Chemphyschem **9**, 994 (2008).

[21] Z. M. Du and N. H. de Leeuw, Surface Science **554**, 193 (2004).

[22] G.-M. Rignanese, J.-C. Charlier, and X. Gonze, Physical Chemistry Chemical Physics **6**, 1920 (2004).

[23] M. Rovere, M. A. Ricci, D. Vellati, and F. Bruni, Journal of Chemical Physics **108**, 9859 (1998).

[24] P. Gallo, M. A. Ricci, and M. Rovere, Journal of Chemical Physics **116**, 342 (2002).

[25] E. B. Moore, E. de la Llave, K. Welke, D. A. Scherlis, and V. Molinero, Physical Chemistry Chemical Physics **12**, 4124 (2010).

[26] J. J. Yang, S. Meng, L. F. Xu, and E. G. Wang, Physical Review B **71**, 035413 (2005).

[27] J. J. Yang and E. G. Wang, Physical Review B **73**, 035406 (2006).

[28] M. C. F. Wander and A. E. Clark, Journal of Physical Chemistry C **112**, 19986 (2008).

[29] D. Argyris, D. R. Cole, and A. Striolo, Journal of Physical Chemistry C **113**, 19591 (2009).

[30] R. Notman and T. R. Walsh, Langmuir **25**, 1638 (2009).

[31] Y. W. Chen and H. P. Cheng, Applied Physics Letters **97**, 161909 (2010).

[32] G. Kresse and J. Furthmüller, VASP, http://cms.mpi.univie.ac.at/marsweb/ (Institut für Materialphysik, Universität Wien, Vienna, Austria, 1999).

[33] P. E. Blöchl, Physical Review B **50**, 17953 (1994).

[34] Y. Wang and J. P. Perdew, Physical Review B **43**, 8911 (1991).

[35] H. J. Monkhorst and J. D. Pack, Physical Review B **13**, 5188 (1976).

[36] N. H. de Leeuw, F. M. Higgins, and S. C. Parker, Journal of Physical Chemistry B **103**, 1270 (1999).

[37] G.-M. Rignanese, A. De Vita, J.-C. Charlier, X. Gonze, and R. Car, Physical Review B **61**, 13250 (2000).

[38] Y. W. Chen, C. Cao, and H. P. Cheng, Applied Physics Letters **93**, 181911 (2008).

[39] V. V. Murashov, Journal of Physical Chemistry B **109**, 4144 (2005).

[40] Y. W. Chen and H. P. Cheng, Journal of Chemical Physics **134**, 114703 (2011).

[41] R. F. W. Bader, *Atoms in Molecules : A Quantum Theory* (Clarendon Press, Oxford ; New York, 1990).

[42] G. Henkelman, A. Arnaldsson, and H. Jónsson, Computational Materials Science **36**, 354 (2006).

[43] D. Pan, L. M. Liu, G. A. Tribello, B. Slater, A. Michaelides, and E. Wang, Physical Review Letters **101**, 155703 (2008).

[44] P. J. Feibelman, Science **295**, 99 (2002).

[45] W. Smith and T. R. Forester, Journal of Molecular Graphics **14**, 136 (1996).

[46] R. T. Cygan, J. J. Liang, and A. G. Kalinichev, Journal of Physical Chemistry B **108**, 1255 (2004).

[47] J. Carrasco, B. Santra, J. Klimes, and A. Michaelides, Physical Review Letters **106**, 026101 (2011).

[48] PWSCF in Quantum Espresso Package, http://www.pwscf.org.

[49] S. Grimme, Journal of Computational Chemistry **27**, 1787 (2006).

[50] V. Barone, M. Casarin, D. Forrer, M. Pavone, M. Sambi, and A. Vittadini, Journal of Computational Chemistry **30**, 934 (2009).

Table 1A. The adsorption and bonding energy of water layers on a silica surface in the H-up state. All energies are in units of meV/Å^2. The (1x1) and (2x1) bare surfaces are denoted as surface I and II. (* Ref. [31])

Surface	E^a_1	E^a_2	E^a_3	E^a_4	E^a_5	E^b_1	E^b_2	E^b_3	E^b_4	E^b_5
I	44.3 *	68.7 *	46.9 *	56.5 *	59.7	1.48 *	1.58 *	1.51 *	1.56	1.57
II	43.9 *	68.8 *	47.0 *	58.3 *		1.43 *	1.44 *	1.56 *	1.56	

Table 1B. The adsorption and bonding energy of water layers on a silica surface in the H-down state. All energies are in units of meV/Å^2. The (1x1) and (2x1) bare surfaces and fully hydroxylated surface are denoted as surface I, II, and III. (* Ref. [31])

Surface	E^a_1	E^a_2	E^a_3	E^a_4	E^a_5	E^b_1	E^b_2	E^b_3	E^b_4	E^b_5
I	46.1 *	48.0	48.2	50.6	53.5	3.84 *	3.26	3.35	5.60	6.28
II	45.6 *	48.4	48.0	51.5		3.01 *	2.70	2.85	5.15	
III	62.2 *	48.5 *	64.1	46.1		34.6*	35.9 *	35.3	36.4	

Table 2. The charge transfer of water layer(s) on a silica surface in the H-down state (positive value indicates gaining electrons). Unit: 10^{-3} e^-. The charge on surface means the charge transferred to the topmost layer of the surface, not including the whole slab.

Surface	monolayer		bilayer		trilayer		quadlayer		pentalayer	
	water	surface	water	surface	water	surface	water	surface	water	surface
I	-18	16	-16	14	-39	21	-226	134	-302	192
II	-16	14	-15	14	-58	33	-234	135		
III	-21	17	-26	23	-38	38	-61	52		

Table 3. The charge redistribution of water layer(s) on a silica surface in the H-down state. Unit: electron.

Surface	monolayer	bilayer	trilayer	quadlayer	pentalayer
I	0.36	0.27	0.42	0.81	0.84
II	0.29	0.23	0.45	0.85	
III	1.85	2.05	2.01	2.13	

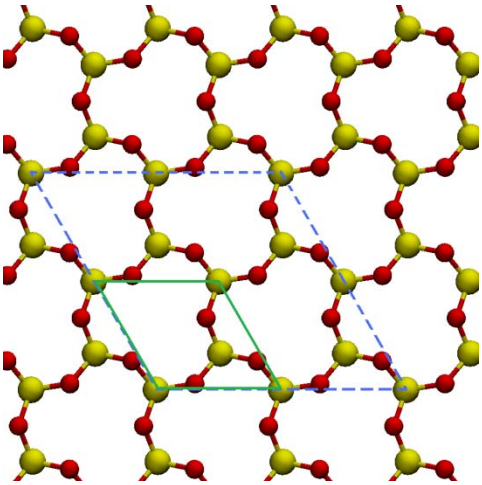

a

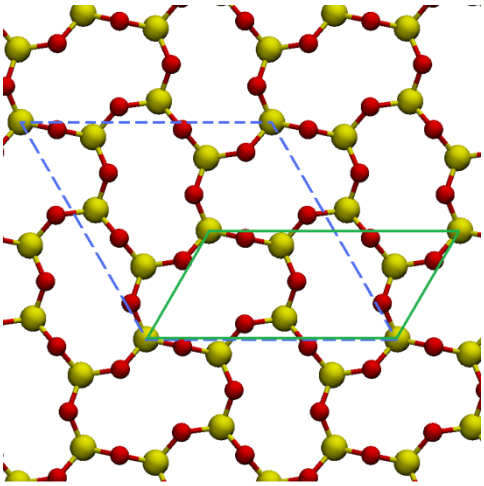

b

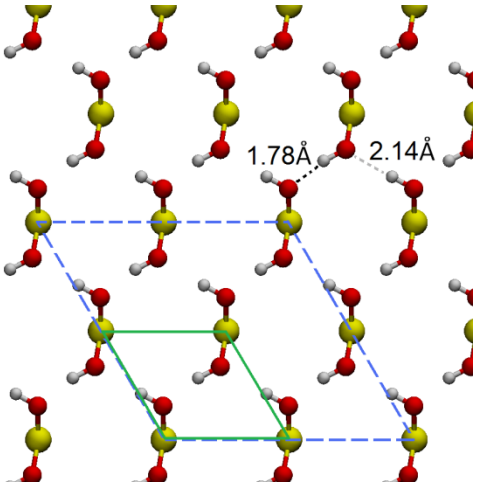

c

Figure 1. (color online) Top views of the (1x1) bare surface (surface I, panel (a)), (2x1) bare surface (surface II, panel (b)), and fully hydroxylated surface (surface III, panel (c)). The silicon atoms are represented as yellow spheres; oxygen in red, and hydrogen in light grey. The hexagonal symmetry blue frame (dashed box) indicates the simulation supercell in the X-Y plane; the green frame (solid box) indicates the minimum unit cell for symmetry.

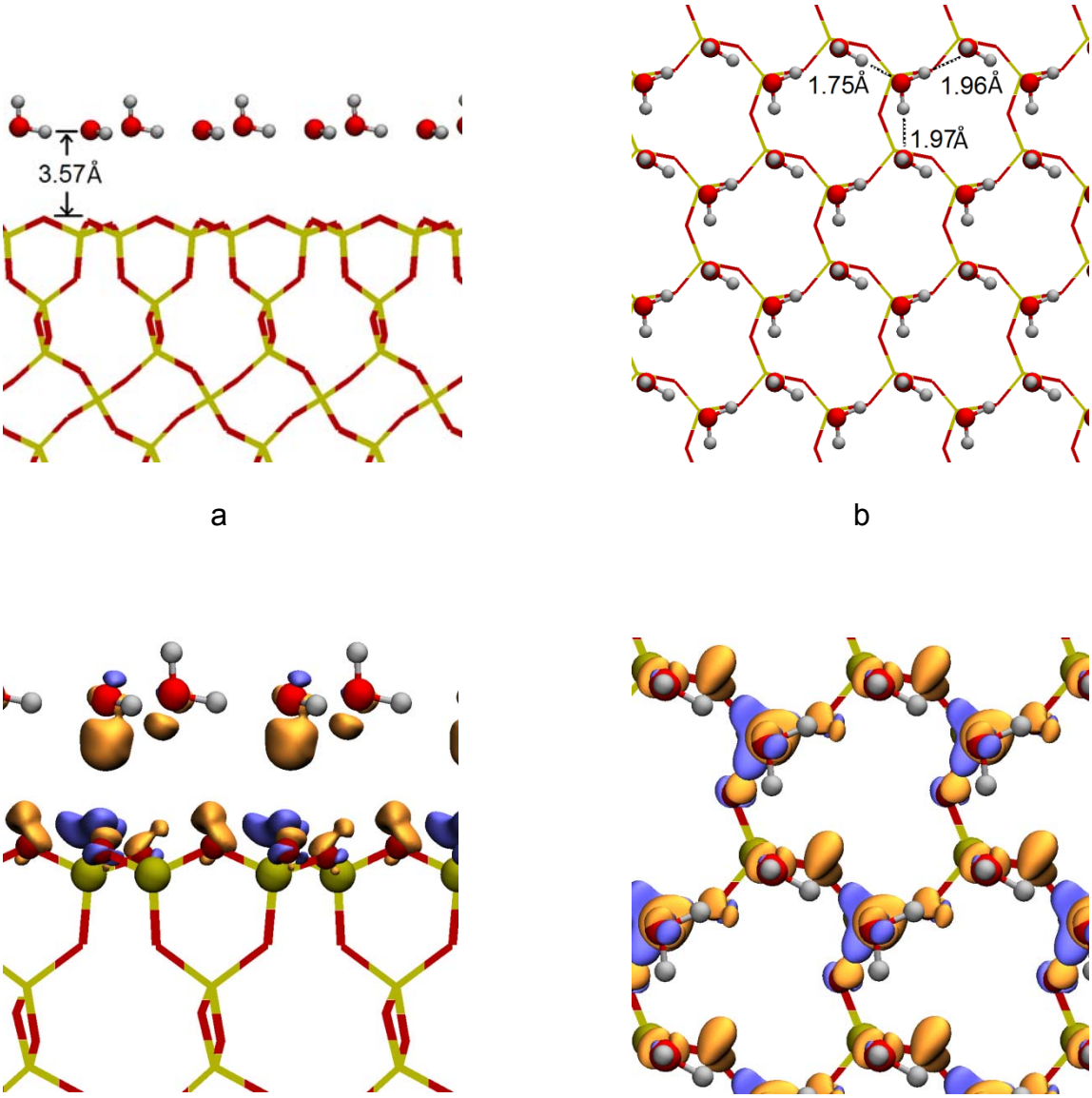

Figure 2. (color online) (a) – (d), Water monolayer adsorbed on surface I in the H-up state. Panels (a) and (b) give the side and top views of the system. Panels (c) and (d) are the side and top views with charge density difference drawn on isosurface of ±0.0005/Å^3. The yellow and blue balloons represent the area with more and less electrons, respectively.

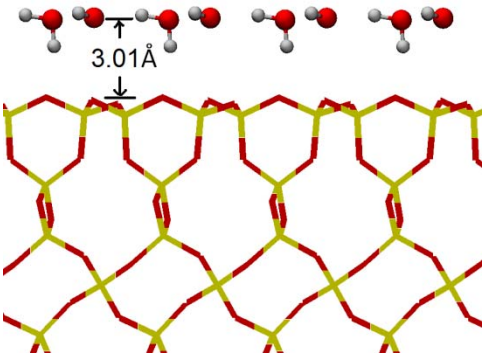

e

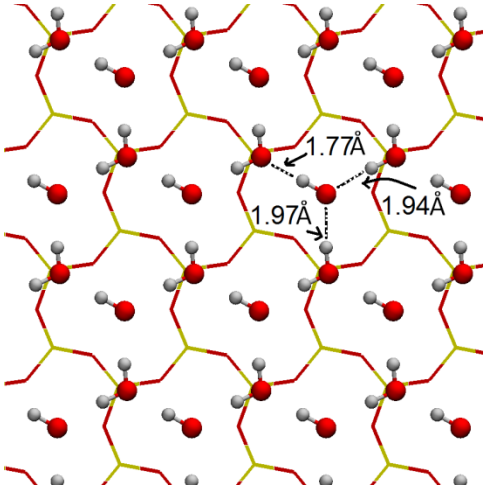

f

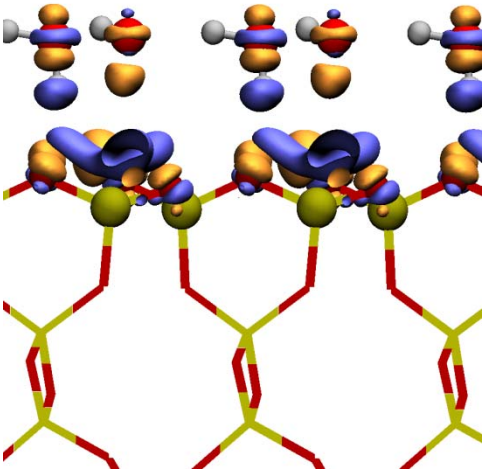

g

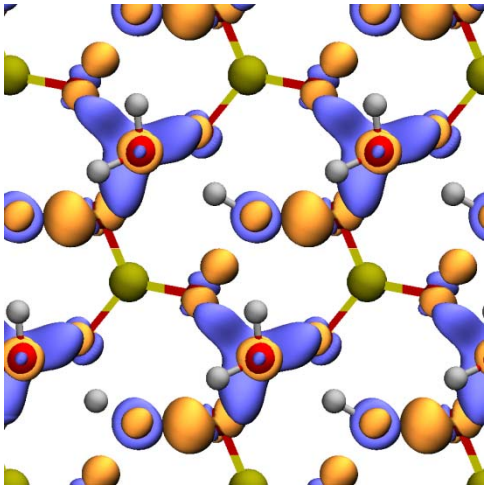

h

Figure 2. (continue) (e) – (h), Water monolayer adsorbed on surface I in the H-down state. Panels (e) and (f) give the side and top views of the system. Panels (g) and (h) are the side and top views with charge density difference drawn on isosurface of ±0.003/Å^3.

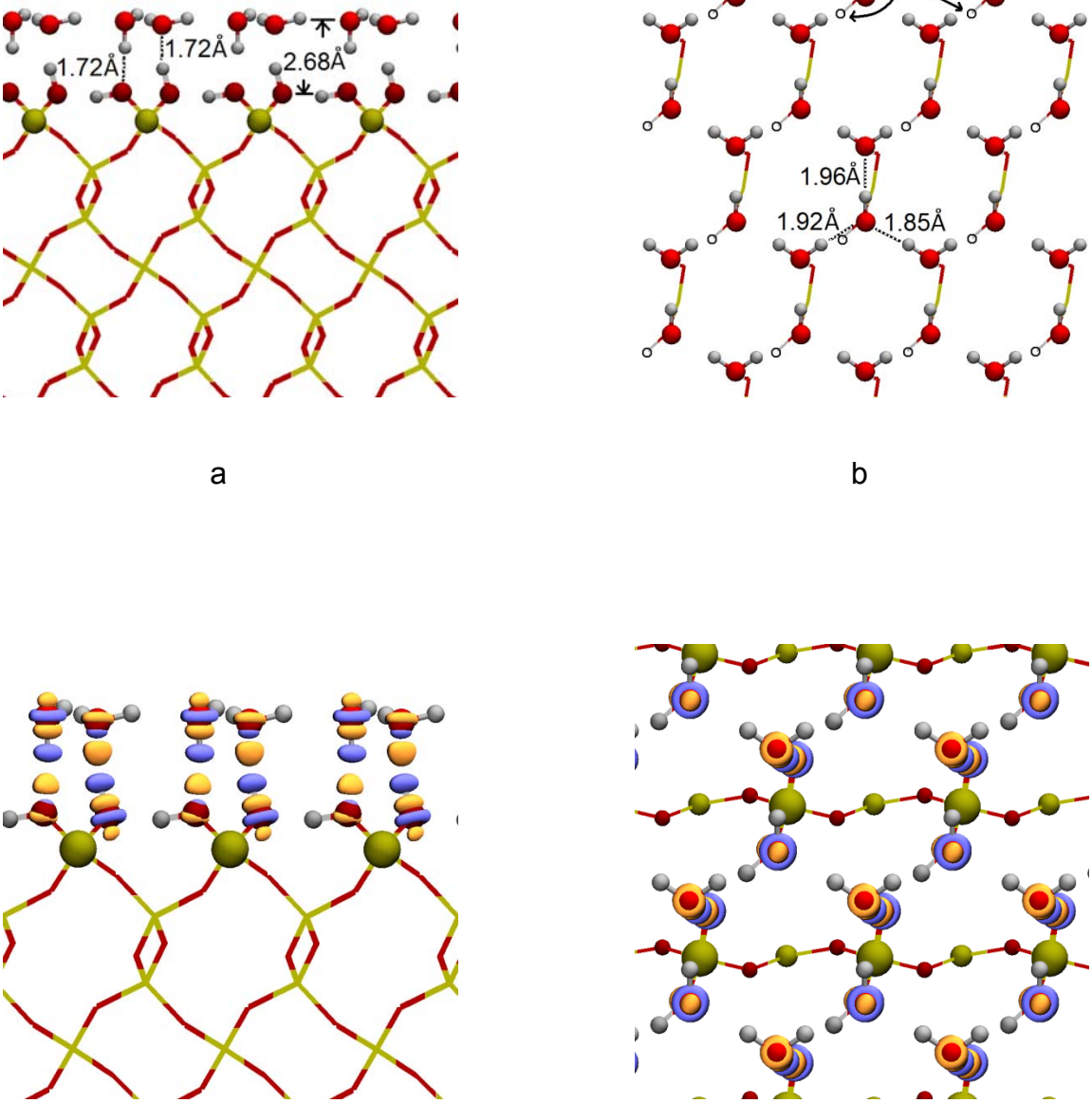

Figure 3. (color online) Water monolayer adsorbed on surface III. Panels (a) and (b) give the side and top views of the system. Panels (c) and (d) are the side and top views with charge density difference drawn on isosurface of ±0.03/Å^3. The marked H atoms in panel (b) are from the hydroxylated surface.

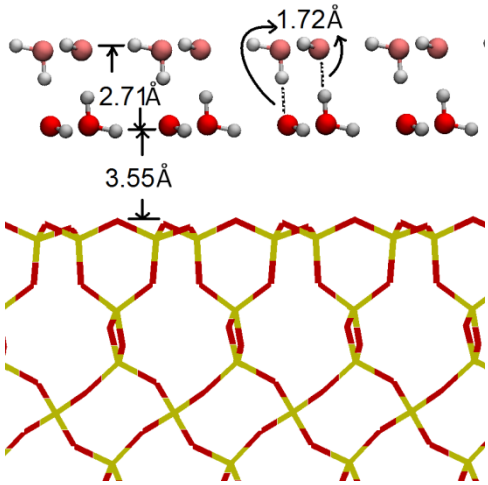

a

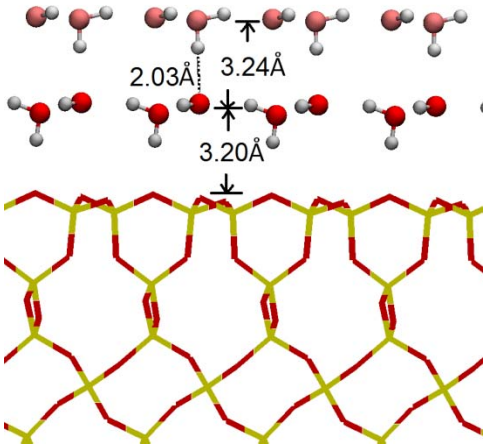

b

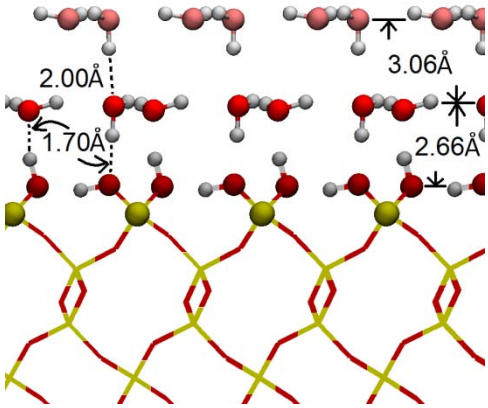

c

Figure 4. (color online) Water bilayer adsorbed on surfaces. Panel (a) shows the side view of H-up state on surface I. Panel (b), H-down state. Panel (c) shows the side view of H-down state on surface III.

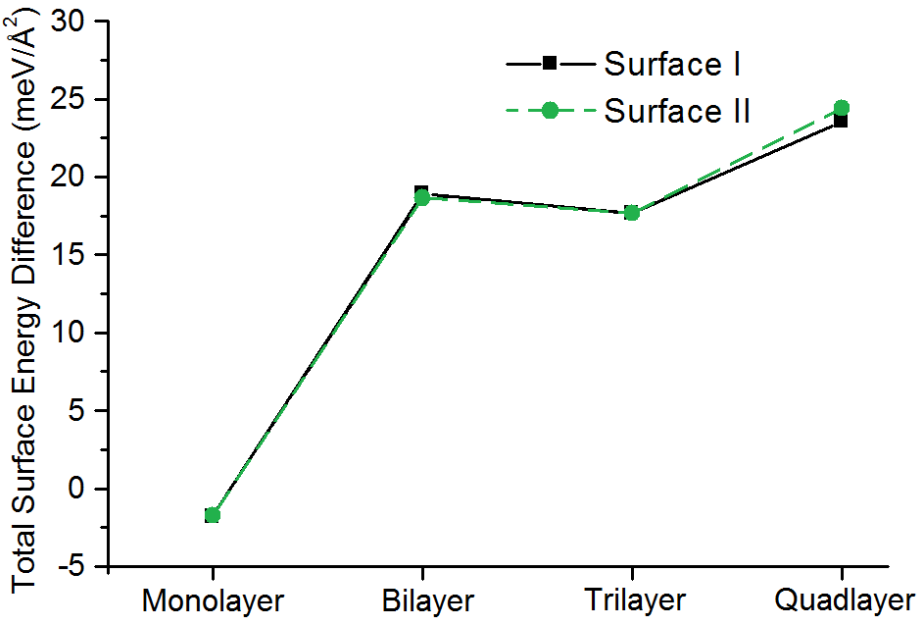

Figure 5. (color online) Total surface energy difference between H-up and H-down state water adsorption on surfaces. The definition is $(E_{total}^{hydrophilic}(n)$ - $E_{total}^{hydrophobic}(n))$/area.

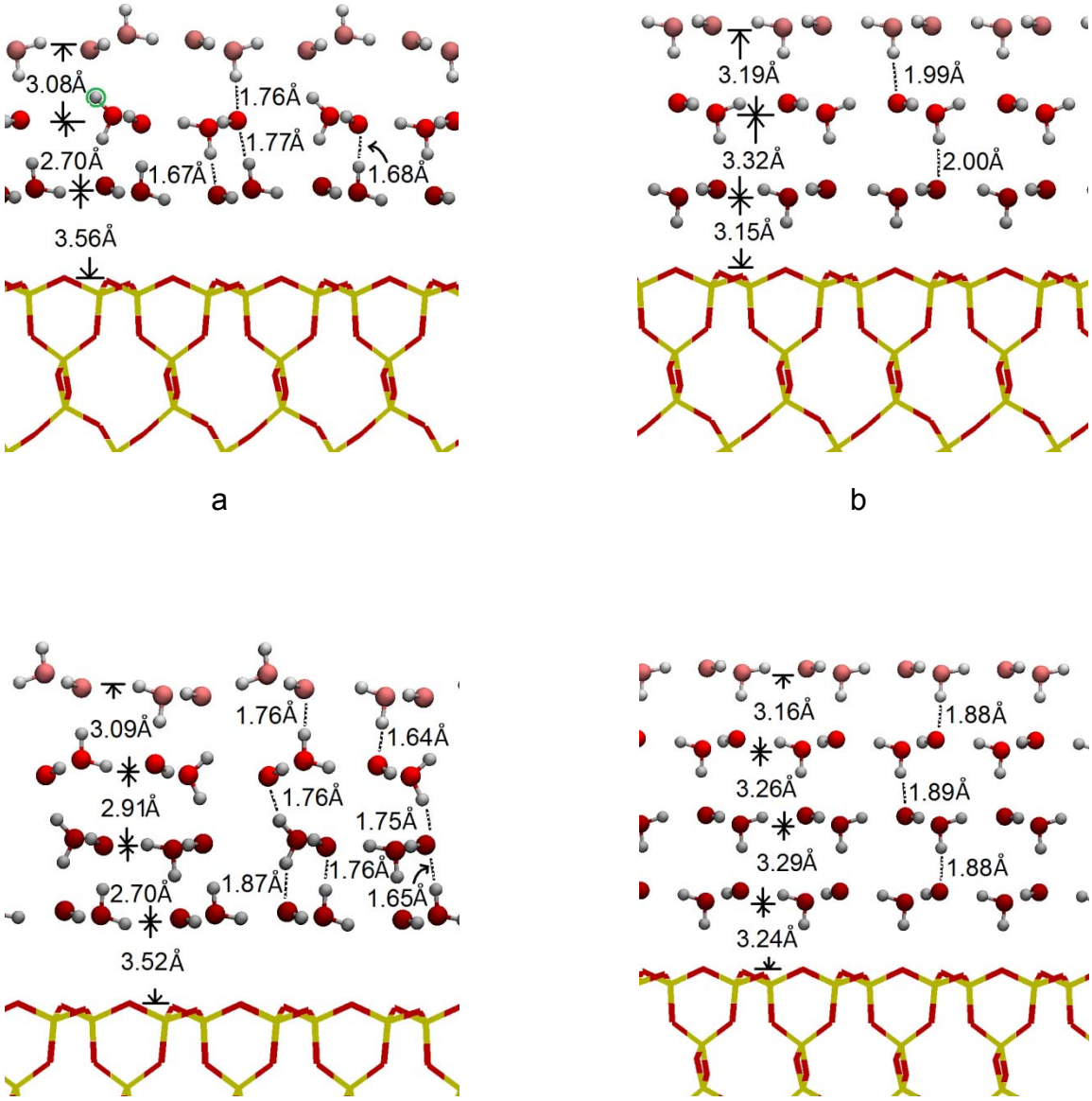

Figure 6. (color online) Water trilayer and quadlayer adsorption on surface I. Panel (a) shows the side view of water trilayer adsorption in H-up state. Panel (b), trilayer in H-down state. Pane (c), quadlayer in H-up state. Pane (d), quadlayer in H-down state. The marked H atom in the panel (a) indicates that its hydrogen bond break in the second water layer.

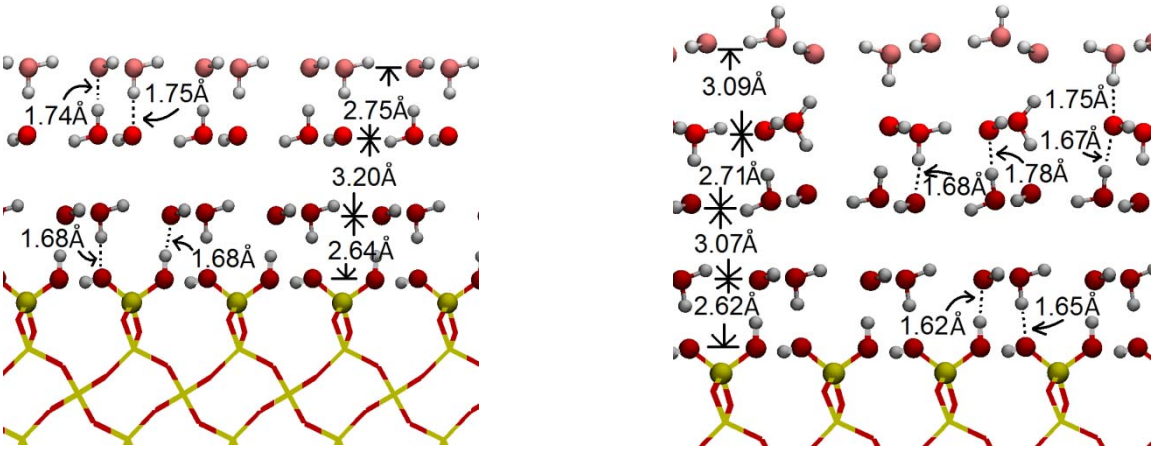

a b

Figure 7. (color online) The side views of water trilayer (panel (a)) and water quadlayer (panel (b)) adsorbed on surface III.

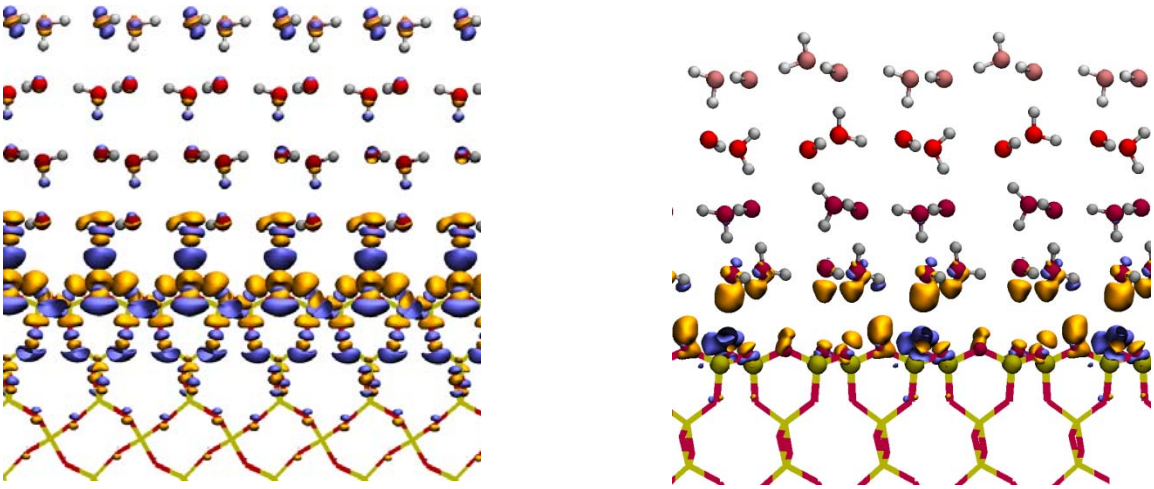

a b

Figure 8. (color online) The side views of water quadlayer adsorbed on surface I with charge density difference distribution. Panel (a) is quadlayer adsorption in H-down state. Panel (b), H-up state. The isosurface of charge density difference is at ±0.002/Å^3 in panel (a); panel (b), ±0.0005/Å^3.

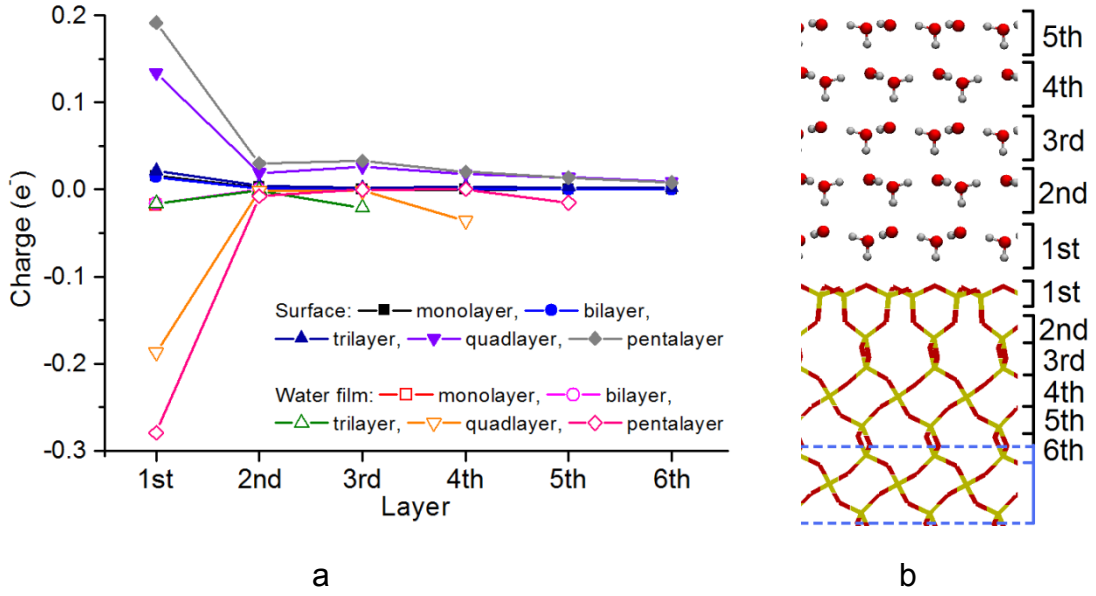

Figure 9. (color online) Panel (a) shows the charge transfer on each water or surface layer in H-down state adsorptions on surface I. Panel (b) depicts the definition of layers in the charge transfer distribution showed in panel (a).The range between two blue dashed lines in panel (b) is the fixed silica layer.

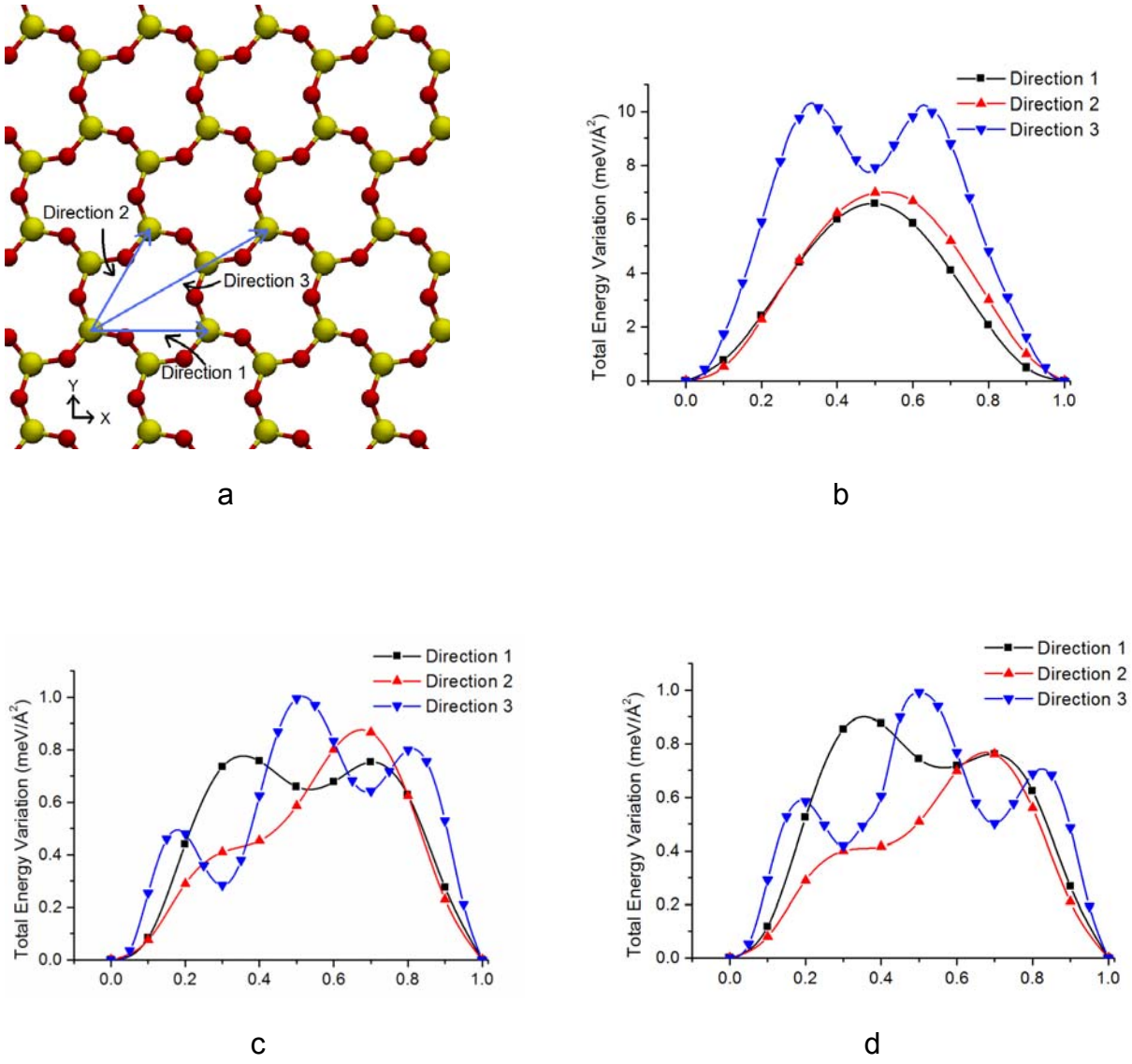

Figure 10. (color online) Panel (a) depicts the three directions for the lateral translations of the water layer on surface I. Panels (b) and (c) show the total energy variation curves for the water monolayer adsorbed on surface I in H-down and H-up states, respectively. Panel (d) shows the total energy variation curves for the water bilayer adsorbed on surface I in the H-up state. In panels (b), (c), and (d), directions 1 and 2 both have ten discrete steps for the total energy variation curve; direction 3 has twenty discrete steps.